NH_3-selective catalytic reduction of NO_x to N_2 over Ceria supported WO_x based catalysts: influence of tungsten content

Imane El Arrouji [1,2], Cuirong Chen [2], Jamil Toyir [3], Cherif Larabi [2], Kai C. Szeto [2], Aimery De Mallmann [2], Mostafa Taoufik [2] and Abdallah Oulmekki [1]

[1] Laboratoire des Procédés, Matériaux et Environnement (LPME), Faculté des Sciences et Techniques de Fès, Université Sidi Mohammed Ben Abdellah, Fès BP. 2202, Morocco; imane.elarrouji@usmba.ac.ma

[2] Institut de Chimie Lyon, Université Lyon 1, CPE Lyon, CNRS, UMR 5265 C2P2, LCOMS, 43 Bd du 11 Novembre 1918, 69616 Villeurbanne Cedex, France ; cuirong.chen@etu.univ-lyon1.fr (C.C.); cherif.larabi@univ-lyon1.fr (C.L.); kai-chung.szeto@univ-lyon1.fr (K.C.S.); aimery.de-mallmann@univ-lyon1.fr (A.d.M.),

[3] Laboratoire des Procédés, Matériaux et Environnement (LPME), Faculté Polydisciplinaire (FP-Taza), Université Sidi Mohammed Ben Abdellah, Taza BP. 1223, Morocco; jamil.toyir@usmba.ac.ma

* Correspondence: mostafa.taoufik@univ-lyon1.fr (M.T.); abdallah.oulmekki@usmba.ac.ma (A.O.); Tel.: +33-472431798 (M.T.)

Abstract: A series of HPW/CeO_2 catalysts generated from 12-tungstophosphoric acid, $H_3PW_{12}O_{40}$ (HPW), supported on ceria and presenting different tungsten loadings (2, 4.5, 9, 16 and 40 wt % W) were prepared and characterized by N_2 physisorption, XRD, IR, Raman, and UV-Vis. The different characterization techniques suggested that low loading of tungsten resulted in mainly isolated sites, while high tungsten loading produced polymeric or tungsten clusters. Those materials exhibited high activity in NH_3 -SCR of NO_x into N_2. Moreover, the series of experiments indicated that low loading in tungsten (2% HPW/CeO_2) displayed the highest activity with a remarkable N_2 selectivity (99%) at medium-high temperature (300-515°C), owing to the high amount of monomeric tungstate coverage on the catalyst surface.

Keywords: DeNOx; 12-tungstophosphoric acid; ceria; tungsten monomeric

1. Introduction

In the last decades, growing interest has been given to developing novel technologies for reducing the harmful gases in environment. Among them are denitration processes for the removal of nitrogen oxides (NO and NO_2 or NO_x). Emitted NO_x is mainly originated from combustion reactions at fairly high temperature, typically in hydrocarbon fuel combustion engines, industrial plants and ammonia combustion power plants [1,2]. Nonetheless, the modifications made to the combustor type or in the combustion processes effectively reduce NOx emissions [3,4]. For example, in currently operated power plants it is possible to improve combustion efficiency up to 99% and reduce pollutant emissions to concentrations lower than 100 ppm just by optimization of injection angles and temperatures at the inlet of combustors [5]. The corresponding optimization of mobile combustion engines has also been conducted. However, due to pursued restriction in NOx emission for mobile transport application, such

engineering optimization remains insufficient to satisfy upcoming regulations. Hence, the urgency to develop more efficient NOx abatement technologies is still essential. NOx removal includes three approaches [6]: (i) direct decomposition of NO_x into O_2 and N_2, NO_x storage reduction (NSR) and (ii) NH_3-selective catalytic reduction (SCR). NO_x selective catalytic reduction (SCR) technology is classified according to the reducing agents used, such as hydrocarbons [7], oxygenated hydrocarbons [8,9], hydrogen [10], or ammonia (or urea) [11,12]. The latter is regarded as an efficient approach to reduce the NO_x emissions due to its high selectivity and relatively simple implementation (without compromising the engine efficiency).

Commercial NH_3-SCR applications typically use V_2O_5-WO_3/TiO_2 as a catalytic converter due to its high performance in a broad temperature window, low cost and an excellent resistance to SO_2 [13]. Nevertheless, the N_2 selectivity decreased at high temperatures, furthermore the release of toxic V_2O_5 at high temperature creates another environmental issue [14]. Therefore, developing high performance and eco-friendly catalysts to perform effective SCR denitration turns out to be a key step for the success of this process.

Tungsten based catalysts attracted more interest owing to their superior acidity, high capacity to suppress undesirable reactions (such as SO2 oxidation) and ability to lead to a better dispersion of the deNOx active sites on the supports [15, 16]. In recent investigations, the incorporation of tungsten to metal oxides like CeO_x, MnO_x, CuO_x,TiO_x, ZrO_x and FeO_x greatly increased the NH_3-SCR activity [17]. Shibo et al. reported that the addition of a small amount of tungsten to $Cu_{0.02}Fe_{0.2}TiO_x$ improves the active surface acidity and increases both the specific surface area and the number of total active sites, which all promote catalytic activity [18]. Additionnally, Wang et al found that the presence of W with MnO_x-TiO_2 forms the active intermediates species responsible for SCR performance [19]. NH_3-SCR on supported catalysts showed high performance with ceria support in association with tungsten, and the redox behavior of ceria and its high capacity to store oxygen were remarkably improved during the SCR process [20]. Several research investigations indicate that the synergic effect is created between the tungsten and Ce^{4+}/Ce^{3+} on the ceria support surface, resulting in a better catalytic conversion [21-23]. In order to further improve and optimize this system, it is crucial to investigate the relationship between the structure of tungsten and the reactivity in NH_3-SCR reactions.

12-tungstophosphoric acid $H_3PW_{12}O_{40}$ (HPW) with the Keggin structure is a cheap and readily available tungsten source and widely applied for both acid and redox-catalyzed reactions [24]. For NH_3-SCR, HPW has been used as precursor on ceria (CeO_2) to improve NH_3 absorption ability after calcination [25]. However, this catalyst shows a poor performance that may be due to low surface area, low dispersion of the tungsten species, and uncontrolled synthesis method. In other studies, Song et al [26]

and Geng et al [22] described the higher performance of ceria grafted HPW which the authors claimed to be related to better NH_3 absorption. Nevertheless, for these systems, the active species controlling the activity are not precisely determined.

In the present study, a series of HPW/CeO_2 (2, 4.5, 9, 16 and 40 wt %) catalysts were synthesized and characterized. The intention is to evaluate the nature of tungsten supported on ceria in NH_3-SCR efficiency. A series of different tungsten loadings allows determining the effect of the dispersion. Simultaneously, this study will also reveal the amount of tungsten required to obtain the optimal catalyst. Special attention is addressed to the structure analysis of the materials using X-ray diffraction, FTIR, and Raman spectroscopy, to the surface characterization by means of N_2 adsorption, in relationship with NH_3-SCR performance.

2. Results and Discussion

2.1. *Characterization of the catalysts*

The catalysts textural properties and tungsten surface density are summarized in Table 1. HPW is a non-porous solid and possesses only a low specific surface area. On the other hand, when deposited on a high surface area ceria (S_{BET} = 247 $m^2.g^{-1}$, surface area determined by the BET approach), a tungsten functionalized material with high specific surface area can be obtained. The surface area and the average pore volume decrease with increasing W loading (Figure S1). This can be explained by a pore blocking mechanism when larger tungsten content is introduced. Thus, the surface is partially inhibited [27]. Changes in surface area and pore volume may affect the catalytic activity of the materials.

Table 1. Textural properties of CeO_2, $H_3PW_{12}O_{40}$ and HPW/CeO_2 (2, 4.5, 9, 16 and 40 wt %).

Catalysts	S_{BET} ($m^2.g^{-1}$)	Pore volume ($cm^3.g^{-1}$)	Surface Density (W at/nm^2)	Average Crystallite Sizes (Å)
$H_3PW_{12}O_{40}$	9	0.019	-	-
CeO_2	247	0.18	-	56
2 % HPW/CeO_2	221	0.17	0.3	57
4.5 % HPW/CeO_2	156	0.16	0.95	67
9 % HPW/CeO_2	141	0.15	2.08	90
16 % HPW/CeO_2	92	0.13	5.69	64
40 % HPW/CeO_2	85	0.08	15.4	58

The HPW shows diffraction peaks characteristics of the Keggin structure, assigned to a triclinic space group P-1 (PDF#00-050-0656). The cubic CeO_2 phase (PDF#04-013-4361) is successfully identified for all the HPW/CeO_2 catalysts. The peaks at 2θ = 28.1°, 33.2°, 47.4°, 56.3°, 52.2° and 69.5° are ascribed to the diffraction lines (111), (200), (220), (331), (222) and (400) respectively [28] (PDF#04-013-4361). In

addition, no characteristic peaks related to the Keggin structure are detected, even at higher tungsten contents, which indicates that the Keggin structure was decomposed into tungsten oxides with an amorphous form or is highly dispersed on CeO_2. Meanwhile, a shift of the ceria peaks was observed, implying that the HPW was successfully impregnated. Based on the Scherrer equation, the average crystallite sizes (Table 1) remain more or less in the same order.

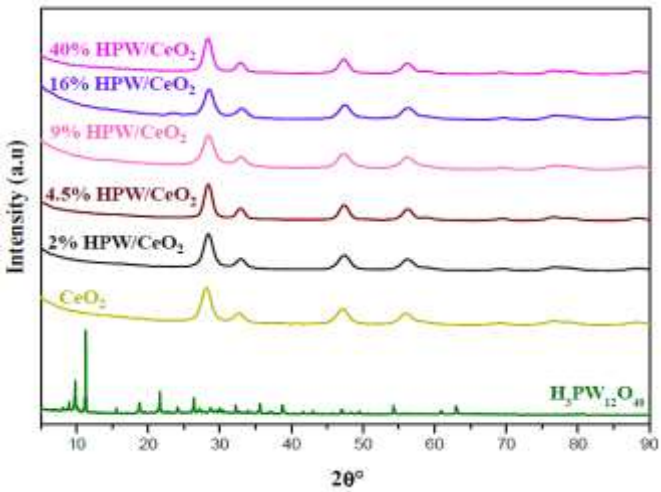

Figure 1. XRD patterns of CeO_2, $H_3PW_{12}O_{40}$ and HPW/CeO_2 (2, 4.5, 9, 16 and 40 wt % W).

FT-IR spectra of the catalysts are shown in Figure 2 and Figure S2. The prepared samples display a peak at 493 cm^{-1}, attributed to Ce-O stretching vibrations [29]. Besides, the rather weak IR signals observed at 947 cm^{-1} and 682 cm^{-1} are assigned to v_s(W=O) and W-O-W moieties respectively. For the catalysts containing 16 and 40 wt% W, a new band appeared at 820 cm^{-1} assigned to asymmetric stretching vibrations of W=O [30]. Compared with the tungstophosphoric acid precursor [31], the HPW in the catalysts did not preserve its Keggin framework, also suggesting that the HPW is decomposed into tungsten oxides after calcination [32].

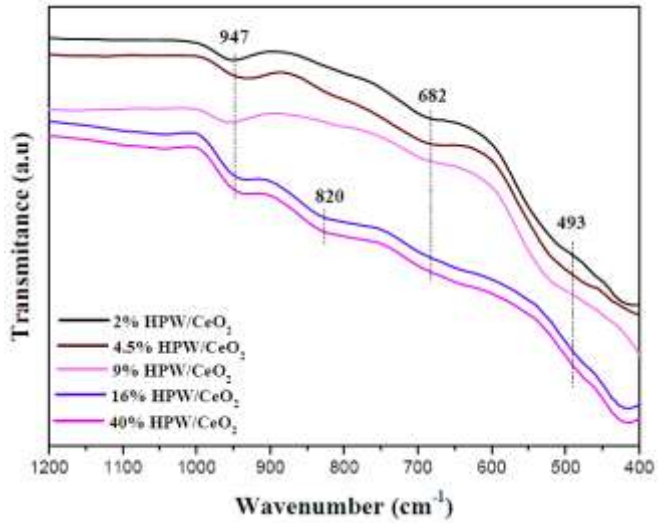

Figure 2. FT-IR spectra of CeO_2, $H_3PW_{12}O_{40}$ and HPW/CeO_2 (2, 4.5, 9, 16 and 40 wt %)

$H_3PW_{12}O_{40}$ Raman spectrum (Figure 3a, lower spectrum) displays the Keggin skeleton characteristic peaks ascribed to symmetric-asymmetric stretching modes of $W^{I}=O_d$ (1011 cm^{-1}), $W^{II}=O_d$ (994 cm^{-1}), P–O_a (906 cm^{-1}), W-O_b-W (522 cm^{-1}) and W-O_c-W (237 cm^{-1}) bonds [33]. For the ceria, an intense symmetrical band at 459 cm^{-1} is ascribed to the F_{2g} vibration mode typical to cubic fluorite phase [34]. Additionally, another band observed at 590 cm^{-1} can probably be instigated by Ce-O symmetry perturbation due to the presence of oxygen vacancies in the CeO_2 structure (Figure S3) [35]. All the supported catalysts show the ceria bands with a slight shift. The I_{Ov}/I_{F2g} values (where I_{F2g} and I_{Ov} are the intensity of F_{2g} (469 cm^{-1}) and O_v (590 cm^{-1}) respectively) reveal the oxygen vacancies contents in the catalysts, which are determined by deconvolution of Raman O_v and F_{2g} peaks. These fairly low values are similar for all catalysts even at higher immobilized W amount (Figure S4, Table S1), indicating that the ceria preserves its surface morphology [36]. In order to further explore the W effect on the ceria support, Raman analysis of tungsten species are shown in 650–1000 cm^{-1} range. It has been reported that the WO_3 bulk, monomeric and polymeric tungstate configurations appeared respectively at 810 cm^{-1}, 930 cm^{-1} and 960 cm^{-1} [23]. In this series of HPW/CeO_2 catalyst, peaks centered around 805–815, 915–930, and 945–960 cm^{-1} are observed. Moreover, for high W content, the mono (915–930 cm^{-1}) and poly-tungstate (945–960 cm^{-1}) appear as one broad peak, which is submitted to a deconvolution operation in order to calculate the contributions of both forms (Figure S4, Table 2). The 2 and 4.5 wt% W/CeO_2 catalysts (0.3 and 0.95 W at/nm^2) show only monomeric tungsten species. When increasing the tungsten loading, the monomeric form would decrease and the ceria surface should gradually be covered by the poly-tungstate oligomeric structure and WO_3 nanoparticles.

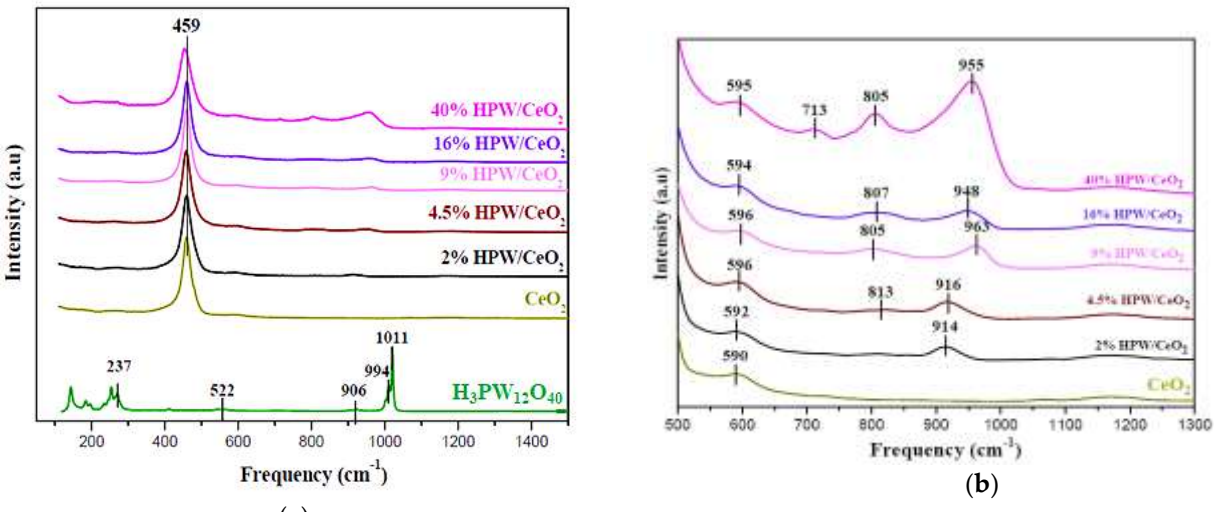

Figure 3. Raman spectra of CeO_2, $H_3PW_{12}O_{40}$, HPW/CeO_2 (2, 4.5, 9, 16 and 40 wt % W) (**a**) and enlarged spectrum for CeO_2 supported tungsten species in the 700-1000 cm^{-1} range (**b**).

Table 2. Structure parameters of HPW/CeO_2 (2, 4.5, 9, 16 and 40 wt % W) catalysts.

Catalysts	W (Monomeric) / W(Mono + Oligo) [1]	WO_3 Nanoparticles [2] (I_{A1g}/I_{F2g})	Estimation of W Monomeric proportion
2% HPW/CeO2	1	0	100 %
4.5% HPW/CeO2	1	0.04	96 %
9% HPW/CeO2	0.67	0.05	64 %
16% HPW/CeO2	0.47	0.06	44 %
40% HPW/CeO2	0.42	0.17	36 %

[1] The area ratios are calculated from the deconvolution of monomeric and oligomeric peaks. [2] The normalized intensity of ν_{A1g} W-O-W (805-813 cm^{-1}) / ν_{F2g} Ce-O (459 cm^{-1}).

The evolution of the bandgap as a function of tungsten loading is determined by UV-visible diffuse reflectance spectroscopy using the O^{2-} to metal charge transfer band (Figure 4). The HPW polytungstate cluster gave an edge energy value (Eg = 3.03 eV) between the isolated tungsten (Na_2WO_4: Eg = 4.89 eV) and WO_x crystals (Eg = 2.3 eV) [37]. The W-O-W bonds number and the electronic delocalization through the WO_x polyhedral neighbors can alter the bandgaps. Nevertheless, the nature of the support oxides also affected the Eg values. CeO_2 itself has a bandgap at 2.7 eV and will inevitably prevent a reliable determination of the bandgap of the catalysts. Hence, it is difficult to probe the tungsten forms on the surface based on UV-vis. Nevertheless, this investigation clearly shows that a higher loading gradually decreases the edge energy (Figure 4b), indicating the presence of more oligomeric/polymeric tungsten species.

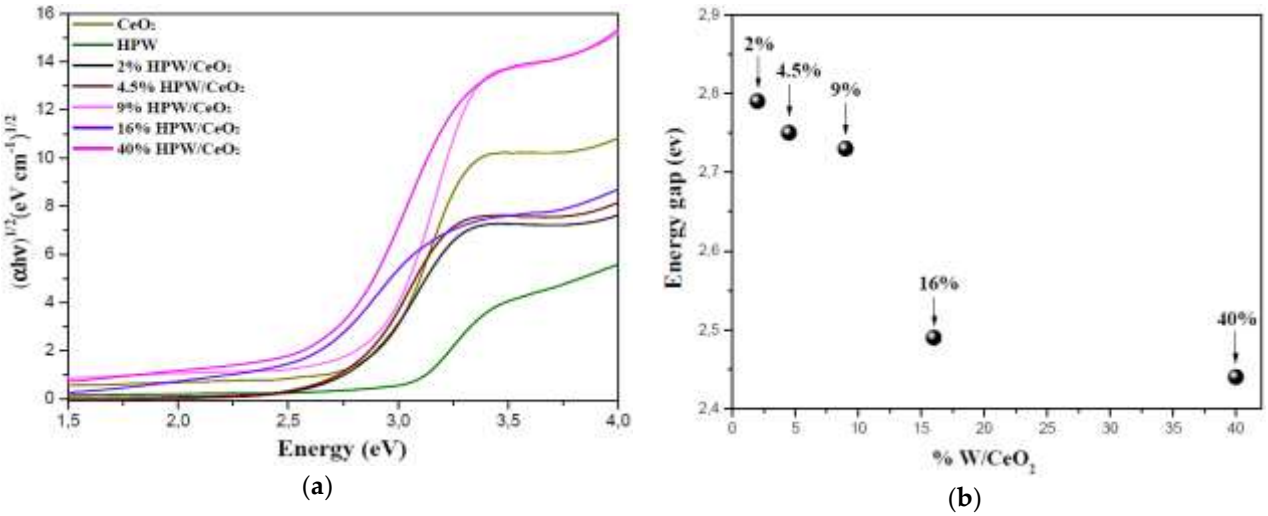

(**a**) (**b**)

Figure 4. (**a**) Tauc plot; (**b**) The energy gaps (Eg) as function of W loadings for HPW/CeO_2 (2, 4.5, 9, 16 and 40 wt %).

The characterization studies carried out for the different catalysts have shown that for low W loadings (2.5 and 4 wt% W), tungsten is mainly present on the ceria surface as monomeric species (Figure 5) while increasing the W loading also leads to oligomeric supported species and some WO_3 bulk. The

estimated proportion of monomeric W species decreasing from 100% (2 wt% W) to 96 (4.5 wt% W), 64 (9 wt% W), 44 (16 wt% W), and 36% (40 wt% W).

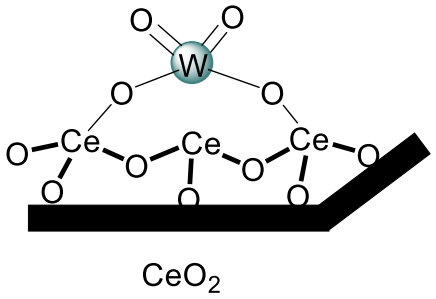

Figure 5. Proposed structure of isolated tungsten bis-oxo on CeO_2.

2.2. *Catalytic activity*

The NO conversion and N_2 selectivity of HPW/CeO_2 with various W contents and 2% HPW/SiO_2 (used for comparison) are displayed in Figure 6 and Figure S6. The NO_x reduction performance of the catalysts decreased in the order 2% HPW/CeO_2 = 4.5% HPW/CeO_2 > 9% HPW/CeO_2> 16% HPW/CeO_2 > 40% HPW/CeO_2 > 2% HPW/SiO_2 > CeO_2. Pure HPW showed almost no activity under the experimental conditions of the reaction due to its important non selective NH_3 oxidation. Modest NH_3-SCR catalytic activity is observed on the pure ceria support, with a NO conversion less than 30% at 400 °C. It is observed that when the HPW is loaded on the ceria, the activity is significantly improved (NO conversion up to 98%). This is probably due to the synergistic effect created between tungsten species and CeO_2. The Ce^{4+} ions on CeO_2 had a good NO_x oxidation ability but a poor NH_3 adsorption [22]. Once loaded 2 and 4.5 wt% of tungsten into the CeO_2, the activity is significantly improved. The 2-4.5% HPW/CeO_2 show an outstanding de-NO_x activity, reaching a maximum NO conversion of 98% across the temperature range 300-515 °C, with a high N_2 selectivity, particularly above 515 °C. Such performance is comparable with existing conventional catalysts [38]. When the tungsten loading was increased to 9 wt%, the catalyst became less efficient with a NOx removal of 98 % at the 296-420 °C interval. The operation temperature interval is also reduced with the insertion of higher amounts of tungsten into ceria. The 16% HPW/CeO_2 and 40% HPW/CeO_2 catalysts showed NO_X conversion of 98% at 286–416 °C and 274–405 °C, respectively. Based on the obtained results, it is worthwhile to note that the NO efficiency is gradually reduced with increasing tungsten loadings to 9, 16, and 40 wt%. Interestingly, the SCR activity is closely dependent on the tungsten loading. It is known for these catalysts types that the modification of ceria with a high amount of tungsten (from HPW acid) enhances the acidity and promotes the NH_3 adsorption at low temperature [22]. This can explain the higher activity observed for highly loaded tungsten catalysts at low temperature, as shown in Figure 6.

However, the opposite trend is observed in the high temperature region. It was found that at higher degree of tungsten loadings, an intense agglomeration of particles was produced, which would cover the active sites. Furthermore, the presence of WO_3 nanoparticles on the ceria surface may affect the nature of these sites. The catalytic performance decreased then from 9% tungsten loading.

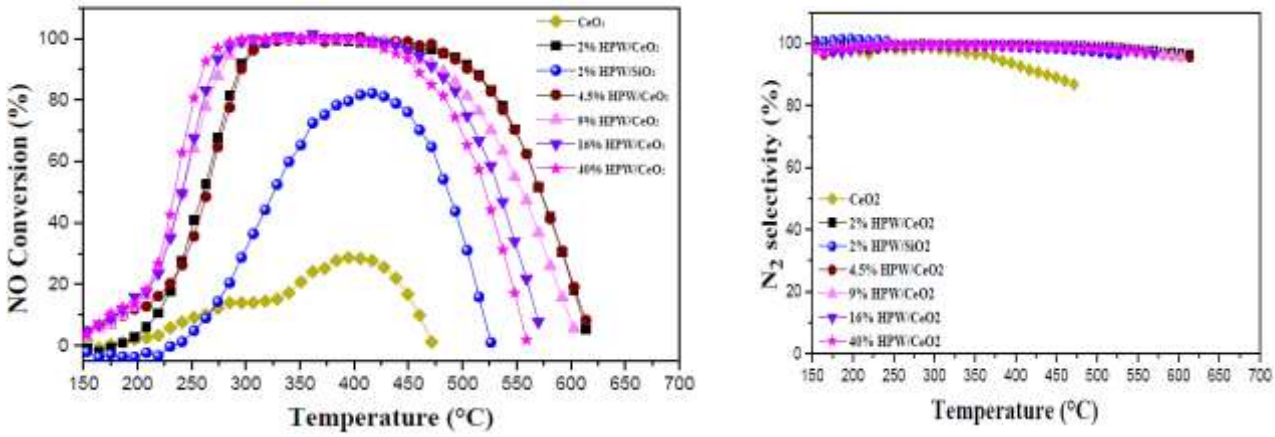

(**a**) (**b**)

Figure 6. NH_3-SCR activity (**a**) and N_2 selectivity (**b**) of HPW/CeO_2 (2, 4.5, 9, 16 and 40% wt) and 2 wt% HPW/SiO_2. Condition: [NH_3] = 350 ppm, [NO] = 300 ppm and GHSV = 30,000 h^{-1}.

The performance of 2% HPW/CeO_2 catalyst is greatly superior to that of 2% HPW/SiO_2 (80% NO conversion is achieved at 420 °C), indicating the favorable synergistic effect created between tungsten and the ceria. In the 2% HPW/CeO_2, the interaction between Ce atom and isolated tungsten (monomeric) (revealed by Raman) produces $W(=O)_2(O\text{-}Ce)_2$ and $W(=O)(O\text{-}Ce)_4$ species [23,39]. This may explain the best activity and the highest stability at high temperature obtained for this 2% HPW/CeO_2 catalyst, where the highest proportion of isolated species is observed. Isolated tungsten species on ceria surface, prepared by an organometallic approach, has recently been demonstrated to be extremely active for NH_3-SCR [40].

The turnover frequencies TOF (calculated based on the converted NO over the total amount of tungsten) were determined to compare the catalytic activity as a function of the tungsten loadings at low (219–253 °C) and high temperatures (525–560 °C). As suggested above, materials with high tungsten loading contain mainly polymeric tungsten species, while samples with low tungsten content comprise mostly isolated species. Hence, a detailed TOF analysis (Figure 7) may provide insights to associate the nature of the active sites with the activity. The TOF is higher at the low temperature region for highly loaded tungsten on ceria, demonstrating that 40% HPW/CeO_2 is more active catalyst. Conversely, in the high temperature region, an increase in the TOF values is observed with lower tungsten contents. These findings indicate that the polymeric tungsten species can readily perform

SCR of NO in the low temperature region, while the isolated tungsten species are more active in the high temperature region. Indeed, the isolate tungstate sites in 2% HPW/CeO_2 would be more accessible to reactants. Moreover, this material shows an acidic behavior, as determined by NH_3-TPD (33.4 µmol/g), a parameter known to improve the catalytic performances even with low W concentration (Figure S6). For this reason, the use of only a small amount of tungsten is enough to achieve the best activity for NO reduction.

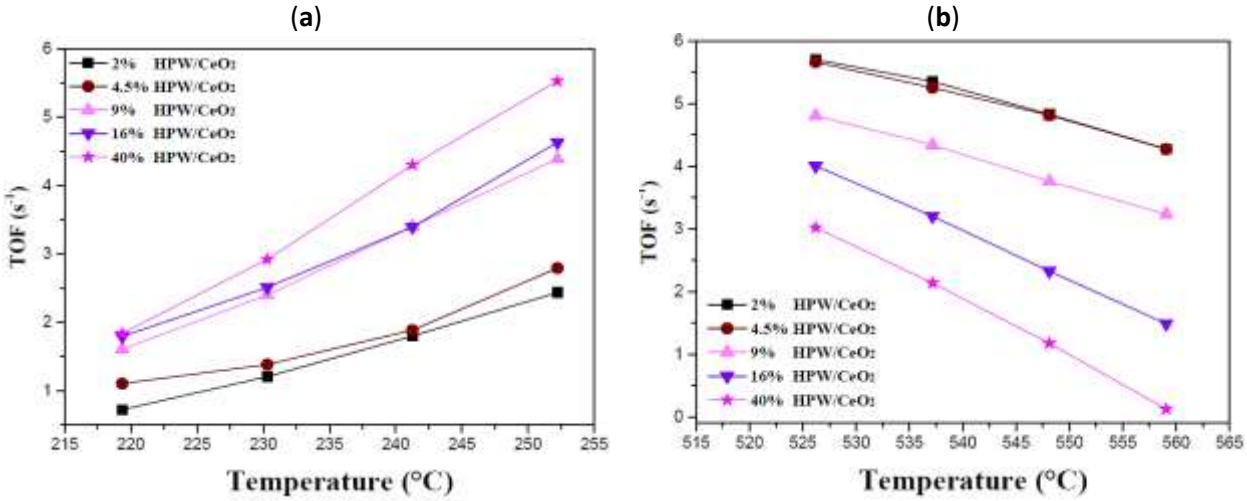

Figure 7. Turnover frequencies TOF of HPW/CeO_2 (2, 4.5, 9, 16 and 40 wt% W) at low (**a**) and high temperatures (**b**).

Additional catalysis experiments have been investigated for 2% HPW/CeO_2 catalyst in the presence of 5% water (Figures S8), reflecting more realistic conditions in combustion engines. The conversion slightly decreased in the presence of water, which is typical. This could be attributed to agglomeration of the tungsten species accelerated by the presence of water. However, the activity and selectivity remained high.

3. Materials and Methods

3.1. Catalysts preparation

A series of HPW/CeO_2 catalysts with increasing tungsten amounts (2, 4.5, 9, 16 and 40 wt %) were synthetized by the wet impregnation method. The solution of tungstophosphoric acid (HPW) in ethanol was added to ceria (CeO_2) at room temperature. The solvent was removed by a rotary evaporator at 30°C. Afterwards, the samples were calcined in air at 500°C for 3h, yelding the catalysts for further characterization and catalytic evaluation.

3.2. Catalysts characterizations

Surface areas were determined with an ASAP 2020 Micromeritics instrument (Norcross, GA, USA) and calculated from the Brunauer, Emmett and Teller (BET) equation. The catalysts were outgassed at 200°C for 4h before the physisorption measurements. The tungsten surface density was calculated based on the following Equation (1):

$$\text{Surface density } (W_{at}/nm^2) = \frac{X_w\, N_A}{S_{BET}\, M_w}$$

where X_w is the loading of the W in the catalyst, N_A is the Avogadro number; M_W is the atomic weight of W and S_{BET} is the surface area of each catalyst.

X-Ray Diffraction (XRD) patterns were performed with a Bruker D8 Advance diffractometer (Billerica, MA, USA), using Cu-$K_{\alpha 1}$ radiation at 40 KV and 40 mA. The refractory lights were collected by a Bruker Lynxeye XE detector for one hour. The diffractograms were analysed by the X'pert highscore software.

DRIFT spectra were recorded with a JASCO FT/IR-4100 spectrometer in the 400-4000 cm^{-1} range, with a 2 cm^{-1} resolution.

Raman spectroscopy was performed on a Labram HR Evo spectrophotometer (from Horiba Jobin-Yvon, Kyoto, Japan) with a green laser diode (λ = 533 nm) using a CDD detector. The spectra were analyzed by the LabSpec software with a spectral resolution < 0.5 cm-1.

UV-visible spectra were carried out with a PerkinElmer Lambda 900 (Waltman, MA, USA). The spectra of the samples were recorded in the 190-850 nm range, at room temperature, using BaSO4 as a reference. Tauc plot was used for determining the gap energy (Eg) by the Kubelka–Munk function in indirect transition, which allows the analysis of crystalline and amorphous compounds. The band gaps (Eg) are estimated from the plot of the tangent line of the $(\alpha h\nu)^{1/2}$ = f (E) curve extrapolated to the abscissa.

Determination of the acidity of the 2%HPW/CeO_2 catalyst by NH_3 desorption: A typical mass of 50 mg of material was used during the experiments. The experiment included four steps: (1) degasification of the sample in Ar at 500 °C for 2 h; (2) adsorption of NH_3 at 120 °C for 1 h; (3) isothermal desorption with Ar at 120 °C until almost no NH_3 was detected; and (4) temperature programmed desorption in Ar at 10 °C/min up to 650 ◦C. The amount of NH_3 in the gas phase was obtained by using an Antaris IGS FTIR (Thermo-Fischer).

3.3. Catalysts measurement

The NH_3-SCR tests were carried out in a quartz continuous-flow reactor using 30 mg catalyst diluted in silicon carbide (SiC). The reaction mixture is composed with 350 ppm NH_3, 10 vol % O_2, 300 ppm NO in

helium with a 300 ml/min total gas flow rate at a velocity of 30,000 h^{-1} (GHSV). The reactor was heated from room temperature to 600 °C (heating rate: 10 °C min^{-1}). The outlet gas concentrations (NH_3, NO, N_2O and NO_2) were analyzed by an Antaris IGS (Thermo-Fischer, Waltham, MA, USA) FT-IR, equipped with a 200 mL gas cell and a DTGS detector. The NO conversion and N_2 selectivity were calculated as follows (Equations (2) and (3)):

$$NO_{\text{conversion}}\ (\%) = 100 \times ([NO]_{in}-[NO_x]_{out}) / [NO]_{in} \quad (2)$$

$$N_{2\ \text{selectivity}}\ (\%) = \frac{[NO]in+[NH_3]in-2[NO_x]out-[NH_3]out-2[N_2O]out}{[NO]in+[NH_3]in-[NO_x]out-[NH_3]out} \quad (3)$$

where $[NO_x] = [NO] + [NO_2]$

4. Conclusions

HPW/CeO_2 catalysts are prepared with different tungsten loadings by wet impregnation method and characterized by N_2 physisorption, XRD, FT-IR, Raman and UV-Vis spectroscopies. The different characterization techniques suggested that low loading of tungsten resulted in mainly isolated sites, while high tungsten loading produced polymeric or tungsten clusters. Those materials exhibited high activity in NH_3-SCR of NO_x into N_2. The materials were further studied for selective reduction reaction of NOx by ammonia. The series of catalysts with different loading allowed further structure-reactivity assignments. Polymeric tungsten species can readily perform SCR of NO in the low temperature region, while the isolated tungsten species are more active in the high temperature region. In terms of catalytic activity, at temperatures higher than 500 °C, the best NO conversion is obtained for the 2 wt% W HPW/CeO_2 catalyst and decreased when increasing the tungsten amount. The enhanced catalytic performance can be attributed to a synergetic interaction between the isolated W and CeO_2, described by monomeric surface moiety expressed as $W(=O)(O\text{-}Ce)_4$ and $W(=O)2(O\text{-}Ce)_2$ on the interface of the 2 wt% W HPW/CeO_2. Such species are believed to improve its stability at high temperature and facilitate the adsorption of reactants. Particularly with this catalyst, a high activity (NO conversion above 98%) is reached at temperature between 300–515 °C, which can be compared with the best catalysts described in the literature with high tungsten loadings [41]. Current findings reveal that the tungsten dispersion will highly affect the NH_3-SCR of NO, in which high dispersion is favorable. The latter has recently been confirmed by a catalytic material based on isolated tungsten species supported on ceria prepared through a delicate organometallic approach. Nevertheless, current work presents a simple synthesis method to access highly dispersed and active catalyst with low loading of tungsten. These result shows that isolated atom materials are highly effective heterogeneous catalysts for future automotive applications [42].

Supplementary Materials: The following are available online: Figure S1: N_2 physisorption isotherms for each catalyst; Figure S2: IR spectra of ceria and HPW; Figure S3: Enlarged picture of the bands attributed to the LO vibration mode of CeO_2 at 500–700 cm^{-1} (Raman spectra); Figure S4: deconvolutions of Raman spectra for each catalyst in the range 300–650 cm^{-1} ; Figure S5: Deconvolutions of Raman spectra for each catalyst in the range 800–1050 cm^{-1} ; Figure S6: NO_x conversion, over HPW as a function of temperature. Feed composition: 300 ppm NO, 350 ppm NH_3 , 5 vol. % H_2O and 10 vol. % O_2 in He; Figure S7: Determination of the acidity of the catalysts 2% HPW/CeO_2 by NH_3 desorption; Figure S8: NO_x conversion and N_2 selectivity obtained with 2% HPW/CeO_2 as a function of temperature with and without water. Feed composition: 300 ppm NO, 350 ppm NH_3, 5 vol. % H_2O and 10 vol. % O_2 in He; Table S1: Oxygen vacancies values of HPW/CeO_2 (2, 4.5, 9, 16 and 40 wt% W) catalysts.

Author Contributions: I.E.A. writing - original draft preparation, data interpretation and experiments. C.C. contributed to the experiments. K.C.S., A.d.M. and C.L. writing and revising. J.T., A.O. and M.T. supervision, project administration and funding acquisition. All authors have read and agreed to the published version of the manuscript.

Funding: This investigation has been supported by the R&D Initiative - Appel à projets autour des phosphates APPHOS – sponsored by OCP (OCP Foundation, R&D OCP, Mohammed VI Polytechnic University, National Center of Scientific and technical Research CNRST, Ministry of Higher Education, Scientific Research and Professional Training of Morocco MESRSFC) under the project entitled ID * CHF-OUL-01/2017. Imane El Arrouji acknowledges a Ph.D. grant from the OCP Foundation for R&D (grant number CHF-OUL-01/2017). CC thanks CSC (China Scholarship Council, grant number 201906740011) for financial support.

Acknowledgments: The authors would like to thank Marc Jeannin and Abdelali Oudriss (LaSIE / La Rochelle University) for Raman experiments.

Conflicts of Interest: The authors declare no conflict of interest

References

1. Franco, M.C.; Rocha, R.C.; Costa, M. Characteristics of NH3/H2/air flames in a combustor fired by a swirl and bluff-body stabilized burner. Proc. Combust. Inst. 2021, 38, 5129–5138.

2. Ariemma, G.B.; Sabia, P.; Sorrentino, G.; Bozza, P.; De Joannon, M.; Ragucci, R. Influence of water addition on MILD ammonia combustion performances and emissions. Proc. Combust. Inst. 2021, 38, 5147–5154.

3. Funke, H.H.; Beckmann, N.; Abanteriba, S. An overview on dry low NO x micromix combustor development for hydrogen-rich gas turbine applications. Int. J. Hydrogen Energy 2019, 44, 6978–6990.

4. Sorrentino, G.; Sabia, P.; Bozza, P.; Joannon, M. De Low-NOx conversion of pure ammonia in a cyclonic burner under locally diluted and preheated conditions. Appl. Energy 2019, 254, 113676.

5. Okafor, E.C.; Somarathne, K.D.K.A.; Hayakawa, A.; Kudo, T.; Kurata, O.; Iki, N. Towards the development of an efficient low-NOx ammonia combustor for a micro gas turbine. Proc. Combust. Inst. 2018, 37, 4597–4606.

6. Liu, S.; Wang, H.; Wei, Y.; Zhang, R.; Royer, S. Morphology-Oriented ZrO2-Supported vanadium oxide for the NH3-SCR process importance of structural and textural properties. ACS Appl. Mater. Interfaces 2019, 11, 22240–22254.

7. Shimizu, K.; Satsuma, A.; Hattori, T. Catalytic performance of Ag-Al2O3 catalyst for the selective catalytic reduction of NO by higher hydrocarbons. Appl. Catal. B Environ. 2000, 25, 239–247.

8. Valanidou, L.; Theologides, C.; Zorpas, A.A.; Savva, P.G.; Costa, C.N. A novel highly selective and stable Ag MgO-CeO2-Al2O3 catalyst for the low-temperature ethanol-SCR of NO. Appl. Catal. B Environ. 2011, 107, 164–176.

9. Popovych, N.; Kirienko, P.; Soloviev, S.; Orlyk, S. Selective catalytic reduction of NOx by C2H5OH over Ag/Al2O3/cordierite: Effect of the surface concentration of silver. Catal. Today 2012, 191, 38–41.

10. Hamada, H.; Haneda, M. A review of selective catalytic reduction of nitrogen oxides with hydrogen and carbon monoxide. Appl. Catal. A Gen. 2012, 421, 1–13.

11. Koebel, M.; Elsener, M.; Kleemann, M. Urea-SCR: A promising technique to reduce NOx emissions from automotive diesel engines. Catal. Today 2000, 59, 335–345.

12. Ciardelli, C.; Nova, I.; Tronconi, E.; Chatterjee, D.; Bandl-konrad, B.; Weibel, M.; Krutzsch, B. Reactivity of NO/NO2–NH3 SCR system for diesel exhaust aftertreatment: Identification of the reaction network as a function of temperature and NO2 feed content. Appl. Catal. B Environ. 2007, 70, 80–90.

13. Huang, X.; Li, S.; Qiu, W.; Chen, Y.; Cheng, J.; Sun, Y.; Bai, G. Effect of organic assistant on the performance of ceria-based catalysts for the selective catalytic. Catalyst 2019, 9, 357.

14. Chen, M.; Jin, Q.; Tao, X.; Pan, Y.; Gu, S. Novel W-Zr-Ox/TiO2 catalyst for selective catalytic reduction of NO by NH3 at high temperature. Catal. Today 2019, 358, 254–262.

15. Kwon, D.W.; Nam, K.B.; Hong, S.C. Influence of tungsten on the activity of a Mn/Ce/W/Ti catalyst for the selective catalytic reduction of NO with NH3 at low temperatures. Appl. Catal. A Gen. 2015, 497, 160–166.

16. Li, C.; Shen, M.; Wang, J.; Wang, J.; Yanping, Z. New Insights into the Role of WO3 in Improved Activity and Ammonium Bisulfate Resistance for NO Reduction with NH3 over V–W-Ce-Ti Catalyst. Ind. Eng. Chem. Res. 2018, 57, 8424–8435.

17. Rui, Y.; Zhenchao, Z.; Shi, C.; Zhang, W. Insight into the synergic effect of Fe-SSZ-13 zeolite and FeMnTiZrOx catalyst with enhanced reactivity in NH -SCR of NOx. J. Phys. Chem. C 2019, 123, 2216–2227.

18. Ma, S.; Zhao, X.; Li, Y.; Zhang, T.; Yuan, F.; Niu, X.; Zhu, Y. Effect of W on the acidity and redox performance of the Cu0.02Fe0.2WaTiOx (a = 0.01, 0.02, 0.03) catalysts for NH3-SCR of NO. Appl. Catal. B Environ. 2019, 248, 226–238.

19. Wang, X.; Li, X.; Zhao, Q.; Sun, W.; Tade, M.; Liu, S. Improved activity of W-modified MnOx-TiO2 catalysts for the selective catalytic reduction of NO with NH3. Chem. Eng. J. 2016, 288, 216–222.

20. Trovarelli, A. Structural and oxygen storage/release properties of CeO2-based solid solutions. J. Crit. Discuss. Curr. Lit. 1999, 20, 263–284.

21. Liang, C.; Junhua, L.; Maofa, G. DRIFT Study on Cerium-Tungsten/Titiania catalyst for selective catalytic reduction of NOx with NH3. Environ. Sci. Technol. 2010, 44, 9590–9596.

22. Geng, Y.; Xiong, S.; Li, B.; Liao, Y.; Xiao, X.; Yang, S. H3PW12O40 grafted on CeO2: A High-performance catalyst for the selective catalytic reduction of NOx with NH3. Ind. Eng. Chem. Res. 2018, 57, 856–866.

23. Kim, G.J.; Lee, S.H.; Nam, K.B.; Hong, S.C. A study on the structure of tungsten by the addition of ceria: Effect of monomeric structure over W/Ce/TiO2 catalyst on the SCR reaction. Appl. Srface Sci. 2020, 507, 145064.

24. Narasimharao, K.; Brown, D.R.; Lee, A.F.; Newman, A.D.; Siril, P.F.; Tavener, S.J.; Wilson, K. Structure-activity relations in Cs-doped heteropolyacid catalysts for biodiesel production. J. Catal. 2007, 248, 226–234.

25. Weng, X.; Dai, X.; Zeng, Q.; Liu, Y.; Wu, Z. DRIFT studies on promotion mechanism of H3PW12O40 in selective catalytic reduction of NO with NH3. J. Colloid Interface Sci. 2016, 461, 9–14.

26. Song, Z.; Zhang, Q.; Ma, Y.; Liu, Q.; Ning, P.; Liu, X. Mechanism-dependent on the different CeO2 supports of phosphotungstic acid modification CeO2 catalysts for the selective catalytic reduction of NO with NH3. J. Taiwan Inst. Chem. Eng. 2017, 71, 277–284.

27. García-fernández, S.; Gandarias, I.; Requies, J.; Güemez, M.B.; Bennici, S.; Auroux, A.; Arias, P.L. New approaches to the Pt/WOx/Al2O3 catalytic system behavior for the selective glycerol hydrogenolysis to 1, 3-propanediol. J. Catal. 2015, 323, 65–75.

28. Ramasamy, V.; Mohana, V.; Rajendran, V. Characterization of Ca doped CeO2 quantum dots and their applications in photocatalytic degradation. OpenNano 2018, 3, 38–47.

29. Kannan, S.K.; Sundrarajan, M.; Green, A. A green approach for the synthesis of a cerium oxide nanoparticle: Characterization and antibacterial activity. Int. J. Nanosci. 2014, 13, 1450018.

30. Kim, D.S.; Ostromecki, M.; Wachs, I.E.; Kohler, S.D.; Ekerdt, J.G. Preparation and characterization of WO3/SiO2 catalysts. Catal. Lett. 1995, 33, 209–215.

31. Javidi, J.; Esmaeilpour, M.; Rahiminezhad, Z.; Dodeji, F.N. Synthesis and characterization of H3PW12O40 and H3PMo12O40 nanoparticles by a simple method. J. Clust. Sci. 2014, 25, 1511–1524.

32. Dong, L.; Hu, Y.; Xu, F.; Lu, D.; Xu, B.; Hu, Z.; Chen, Y. A study on the surface properties of ceria-supported tungsten and copper oxides. J. Phys. Chem. B 2000, 104, 78–85.

33. Marcì, G.; García-lópez, E.I.; Rita, F.; Liotta, L.F.; Palmisano, L. General Enhanced (photo) catalytic activity of Wells-Dawson (H6P2W18O62) in comparison to Keggin (H3PW12O40) heteropolyacids for 2-propanol dehydration in gas-solid regime. Appl. Catal. A Gen. 2016, 528, 113–122.

34. Castro, D.; Sigoli, F.A.; Mazali, I.O. Reversible Oxygen Vacancy Generation on Pure CeO2 Nanorods Evaluated by in Situ Raman Spectroscopy. J. Phys. Chem. C 2017, 121, 12928–12935.

35. Farias, M.D.D.; Nguyen-thanh, D.; Fraga, M.A. Environmental Discussing the use of modified ceria as support for Pt catalysts on water-gas shift reaction. Appl. Catal. B Environ. 2010, 93, 250–258.

36. Li, X.; Wang, Z.; Sun, J.; Oh, R.; Feng, J.; Shi, D.; Zhao, W.; Liu, S. Influence of CeO2 morphology on WO3/CeO2 catalyzed NO selective catalytic reduction by NH3. J. Energy Inst. J. 2020, 93, 1–8.

37. Howell, J.; Li, Y.; Bell, A.T. Propene metathesis over supported tungsten oxide catalysts: A study of active site formation. ACS Catal. 2016, 6, 1–32.

38. Li, Z.; Li, J.; Liu, S.; Ren, X.; Ma, J.; Su, W. Ultra hydrothermal stability of CeO2-WO3/TiO2 for NH3-SCR of NO compared to traditional V2O5-WO3/TiO2 catalyst. Catal. Today 2015, 258, 11–16.

39. Gu, Y.; Cai, T.; Gao, X.; Xia, H.; Sun, W.; Zhao, J.; Dai, Q.; Wang, X. Catalytic combustion of chlorinated aromatics over WOx/CeO2 catalysts at low temperature. Appl. Catal. B Environ. 2019, 248, 264–276.

40. Larabi, C.; Chen, C.; Merle, N.; Charlin, M.; Szeto, K.C.; De Mallmann, A.; Benayad, A.; Ben Tayeb, K.; Kaddouri, A.; Nguyen, H.P.; et al. Well-defined surface tungstenocarbyne complex through the reaction of [W(≡CtBu)(CH2tBu)3] with CeO2: A highly (active) and stable precatalyst for NOx reduction with NH3. New J. Chem. 2021, 45, 12024–12032.

41. Ma, Z.; Weng, D.; Wu, X.; Si, Z. Effects of WOx modification on the activity, adsorption and redox properties of CeO2 catalyst for NOx reduction with ammonia. J. Environ. Sci. 2012, 24, 1305–1316.

42. Higashi, A.; Shougo, B. Towards dense single-atom catalysts for future automotive applications. Nat. Catal. 2019, 2, 590–602.